

LETTER TO THE EDITOR

LoCuSS: Probing Galaxy Transformation Physics with Herschel[★]

G. P. Smith¹, C. P. Haines¹, M. J. Pereira², E. Egami², S. M. Moran³, E. Hardegree-Ullman⁴, A. Babul⁵, M. Rex², T. D. Rawle², Y.-Y. Zhang⁶, A. Finoguenov^{7,8}, N. Okabe⁹, A. J. R. Sanderson¹, A. C. Edge¹⁰, and M. Takada¹¹

(Affiliations can be found after the references)

Received March 31, 2010; Accepted May 19, 2010

ABSTRACT

We present an early broad-brush analysis of *Herschel*/PACS observations of star-forming galaxies in 8 galaxy clusters drawn from our survey of 30 clusters at $z \approx 0.2$. We define a complete sample of 192 spectroscopically confirmed cluster members down to $L_{\text{TIR}} > 3 \times 10^{10} L_{\odot}$ and $L_K > 0.25 L_{\odot}$. The average K -band and bolometric infrared luminosities of these galaxies both fade by a factor of ~ 2 from clustercentric radii of $\sim 2r_{200}$ to $\sim 0.5r_{200}$, indicating that as galaxies enter the clusters ongoing star-formation stops first in the most massive galaxies, and that the specific star-formation rate (SSFR) is conserved. On smaller scales the average SSFR jumps by $\sim 25\%$, suggesting that in cluster cores processes including ram pressure stripping may trigger a final episode of star-formation that presumably exhausts the remaining gas. This picture is consistent with our comparison of the *Herschel*-detected cluster members with the cluster mass distributions, as measured in our previous weak-lensing study of these clusters. For example, the spatial distribution of the *Herschel* sources is positively correlated with the structures in the weak-lensing mass maps at $\sim 5\sigma$ significance, with the strongest signal seen at intermediate group-like densities. The strong dependence of the total cluster IR luminosity on cluster mass – $L_{\text{TIR}} \propto M_{\text{virial}}^2$ – is also consistent with accretion of galaxies and groups of galaxies (i.e. the substructure mass function) driving the cluster IR luminosity. The most surprising result is that roughly half of the *Herschel*-detected cluster members have redder S_{100}/S_{24} flux ratios than expected, based on the Rieke et al. models. On average cluster members are redder than non-members, and the fraction of red galaxies increases towards the cluster centers, both of which indicate that these colors are not attributable to systematic photometric errors. Our future goals include to interpret physically these red galaxies, and to exploit this unique large sample of clusters with unprecedented multi-wavelength observations to measure the cluster-cluster scatter in S0 progenitor populations, and to interpret that scatter in the context of the hierarchical assembly of clusters.

Key words. galaxies: clusters galaxies: evolution galaxies: star formation Infrared: galaxies

1. Introduction

Lenticular galaxies (hereafter S0s) are mainly found in the cores of galaxy clusters at low redshift (e.g. Dressler et al. 1997; Smith et al. 2005; Postman et al. 2005). There is a broad consensus that they are the descendants of gas rich spiral galaxies that have been accreted from the surrounding filamentary structure. However the physics of how spirals are transformed into S0s remains largely unconstrained, with numerous “S0 progenitor” populations (e.g. Moran et al. 2006; Poggianti et al. 2000; Geach et al. 2006; Haines et al. 2009a – hereafter H09a) and physical processes (e.g. Gunn & Gott 1972; Moore et al. 1999) discussed in the literature.

The broad range of cluster-centric radii at which various S0 progenitors are found reflects the fact that different physical processes act in different environments, for example ram pressure stripping is more effective closer to cluster centers where the intracluster medium (ICM) is denser, and galaxy-galaxy merging is more effective in galaxy groups that are falling into the cluster than in the cluster cores. Moreover, the observational signatures of S0 progenitors are diverse, ranging in wavelength from ultraviolet (UV) emission from A stars in galaxies whose star-formation (SF) has been recently quenched, through optical spectral features including Balmer absorption lines, to mid/far-infrared (IR) emission from dust heated by SF (e.g. Moran et al. 2007; Poggianti et al. 2000; Haines et al. 2009b).

Mid- and far-IR properties of cluster galaxies have been studied previously with *IRAS* (e.g. Leggett et al. 1987; Doyon & Joseph 1989), *ISO* (see Metcalfe et al. 2005 for a review), and *Spitzer* (e.g. Geach et al. 2006; Fadda et al. 2008; Haines et al. 2009a,b; Bai et al. 2009). A key result from these IR studies is that a significant fraction of the total SF in galaxy clusters is obscured by dust. The inferred levels of SF naturally fit the hypothesis that bulge dominated S0s are descended from late-type spirals. It has also been suggested that dusty S0 progenitors are more common in dynamically active, i.e. merging, galaxy clusters than in so-called “relaxed” clusters (e.g. Metcalfe et al. 2005; Geach et al. 2006; Miller et al. 2006). However it has thus far been difficult to test this idea robustly because the intrinsic scatter in levels of SF in clusters appears to be large, (as noted by Kodama et al. 2004), and the sample sizes observed to date are small (i.e. $\lesssim 2$) within any given redshift bin – although see H09a for a recent counter-example.

We are therefore conducting a systematic wide-field survey of a large statistically well-defined sample of galaxy clusters in a narrow redshift slice at $z \approx 0.2$, as part of the Local Cluster Substructure Survey (LoCuSS¹). Our goals are to compile a complete inventory of S0 progenitors using data from the far-UV to far-IR, and to relate these populations to the underlying gas physics and hierarchical structure of the host galaxy clusters. We aim to delineate the different physical processes responsible for galaxy transformation in clusters and their surrounding large scale structure, and thus constrain the amplitude of the different physical pathways from spiral to S0 morphology, and how these

[★] Herschel is an ESA space observatory with science instruments provided by European-led Principal Investigator consortia and with important participation from NASA.

¹ <http://www.sr.bham.ac.uk/locuss/>

relate to the dynamical state of the clusters. Our Open Time Key Programme observations with *Herschel* (Pilbratt et al., 2010), supplemented by existing *Spitzer* mid-IR observations provide the all-important measurements of the bolometric IR luminosity and mid/far-IR colors of dust-reddened/obscured S0 progenitors.

We assume $H_0=70\text{km s}^{-1}$, $\Omega_M=0.3$, $\Omega_\Lambda=0.7$. In this cosmology 1kpc at $z=0.2$, subtends $0.3''$. All cluster masses and radii relative to an over-density are derived from the weak-lensing analysis of Okabe et al. (2010; hereafter Ok10).

2. Survey Design

Our survey goals include understanding the physical reasons for the large cluster-cluster variations in SF rate (SFR), and the full range of physical processes responsible for transforming spiral galaxies into S0s. We therefore require a large sample of clusters in order to sample thoroughly the underlying cluster population and the various S0 progenitor populations that they host. Our sample of 30 clusters therefore will allow us to study, for example, how total integrated cluster SFRs depend on global cluster properties such as cool core strength, and substructure fraction, in $\sim 3\text{--}6$ cluster bins with $\sim 5\text{--}10$ clusters per bin. Based on previous IR and UV studies of S0 progenitors, we expect $\sim 30\text{--}50$ such objects per cluster. Our sample of 30 clusters should therefore deliver a sample of ≥ 1000 S0 progenitors.

With current observing facilities and observed cluster samples, this study is prohibitively expensive at high redshift because of the requirement for wide-field and moderately deep data on a large sample. We therefore concentrate on clusters at $z\approx 0.2$; at this redshift gravitational lensing is an efficient probe of the dark matter distribution in the cluster in-fall regions using Suprime-CAM on the Subaru telescope, and yet follow-up *Herschel* observations of a sample of 30 clusters are feasible.

The cluster sample is a subset of those in the *ROSAT* All-sky Survey catalogs (Ebeling et al. 1998, 2000; Böhringer et al. 2004) that satisfy the following criteria: $0.15 < z < 0.3$, $n_H < 7 \times 10^{20} \text{cm}^{-2}$, and $-70^\circ < \delta < +70^\circ$, and that were observable with Subaru/Suprime-CAM on the nights assigned to us (Ok10). The sample is therefore blind to the thermodynamic, and hierarchical assembly history of the clusters, other than the use of X-ray luminosity as a proxy for mass-selection. The distribution of the X-ray luminosities of clusters in our sample is statistically indistinguishable from that of a volume-limited sample satisfying $L_X E(z)^{-2.7} > 4.2 \times 10^{44} \text{erg s}^{-1}$, where the scaling of L_X with $E(z)^2 = \Omega_M (1+z)^3 + \Omega_\Lambda$ approximates mass-selection following Popesso et al. (2005) – see Ok10 for more details.

Our multi-wavelength observations of this sample (§3) span at least a clustercentric radius of 12.5arcmin on the sky, equating to $\sim 1.5 r_{200}$ for a typical cluster in our sample. This physical field of view is sufficiently large to probe all of the physical processes expected to play a role in galaxy transformation (Fig. 1).

3. Observations and Data Analysis

The 8 clusters discussed in this letter were observed with the Photodetector Array Camera and Spectrometer (PACS; Poglitsch et al. 2010) across a $25' \times 25'$ field of view at 100 and $160 \mu\text{m}$ in scan map mode at 20arcsec/s in November and December 2009. Each cross scan was repeated 7 times, giving a total exposure time of 93.2s/pix . We first processed the data using standard HIPE routines (Ott 2010). Then all sources detected at $\geq 2.5\sigma$ in the first pass reduced data were masked using $15''$ circular apertures, and the data were high pass filtered with a

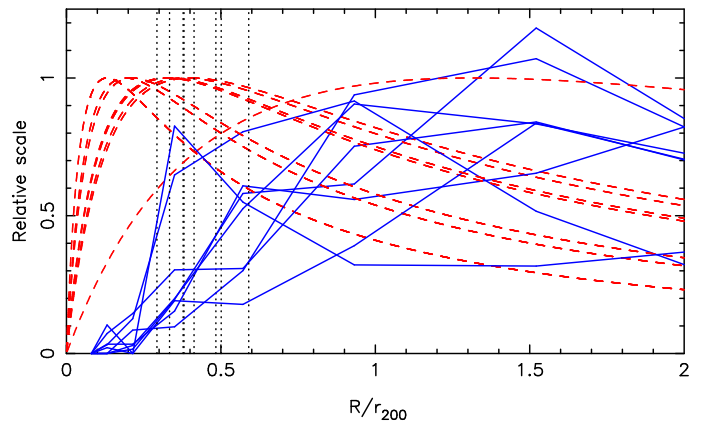


Fig. 1. This figure shows simple physically well-motivated models for the relative strength of ram pressure stripping, harassment, and galaxy-galaxy merging in the eight clusters discussed in this letter. The vertical black dotted lines show the stripping radius for each cluster – the radius within which ram pressure is able to strip a disk galaxy with rotation speed of 160km s^{-1} . This calculation combines Sanderson et al.’s (2009) *Chandra*-based gas density profiles with Ok10’s weak lensing-constrained NFW density profiles, and assumes that the typical radial velocity of infalling galaxies is $0.9V_C$ at the virial radius where V_C is the circular velocity of the cluster dark matter halo, following the analytic model of McCarthy et al. (2008). Red dashed curves show the relative efficiency of harassment, based on the harassment rate of $f_H \propto \rho_{\text{gal}} r^2$ (Moore et al. 1998), assuming that the total mass distribution traces the galaxy density (Lin et al. 2004) – i.e. we substitute ρ_{NFW} from Ok10 for ρ_{gal} . The galaxy-galaxy merger rate is traced by the solid blue curves, which show the radial number density profile of galaxies that inhabit group-like environments, i.e. a 3-dimensional galaxy density of $2 \leq \rho_{3D} \leq 10 \text{Mpc}^{-3}$, derived from our near-IR photometry (H09a) and large spectroscopic catalogs (Hardegree-Ullman et al. in prep.).

filter 25 and 30 frames wide at $100 \mu\text{m}$ and $160 \mu\text{m}$ respectively. The final maps were then constructed using the PHOTPROJECT routine. The angular resolution of the final reduced frames is $6.8''$ at $100 \mu\text{m}$ and $11.4''$ at $160 \mu\text{m}$.

Sources were extracted using SExtractor, employing circular apertures of $12''$ and $16''$ diameter at 100 and $160 \mu\text{m}$. The point spread function in the $100 \mu\text{m}$ frame is slightly de-graded from that derived from the PACs calibration maps of Vesta, due to imperfect spatial calibration within scans where bright sources cannot be used to register the individual exposures. We therefore applied an empirical aperture correction of 1.65 ± 0.03 , based on brightest isolated sources in the $100 \mu\text{m}$ maps. The standard Vesta aperture correction of 1.675 was applied at $160 \mu\text{m}$. The 90% completeness limits are 18mJy at $100 \mu\text{m}$ and 28mJy at $160 \mu\text{m}$. Calculation of the total IR luminosities ($8 < \lambda < 1000 \mu\text{m}$) discussed in §4 are described by Haines et al. (2010).

We also use our wide-field data from *Spitzer*/MIPS ($24 \mu\text{m}$; H09a), UKIRT/WFCAM (*J/K*-bands; H09a), *Chandra* (Sanderson et al., 2009), and Subaru/Suprime-CAM (*V/i'*-bands; Okabe & Umetsu 2008; Ok10). We have spectroscopically identified 92% of the sources down to the $100 \mu\text{m}$ detection threshold using MMT/Hectospec (Fabricant et al. 2005), in addition to securing $\sim 200\text{--}300$ cluster galaxy redshifts per cluster (Hardegree-Ullman et al., in prep.).

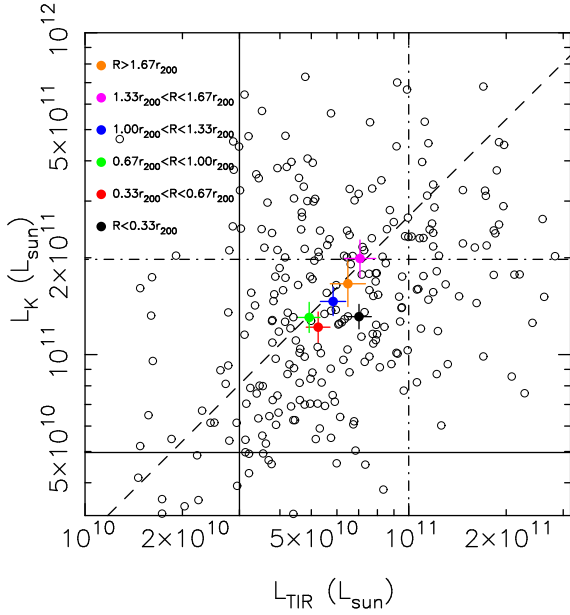


Fig. 2. K -band luminosity (L_K) versus total infrared luminosity (L_{TIR}) for the *Herschel*-detected cluster members, plotted as open circles. The horizontal and vertical solid lines show the completeness limits of our MMT/Hectospec spectroscopic survey and our *Herschel* photometry respectively; the horizontal and vertical dot-dashed lines show L_K^* from Lin et al. (2004) and the definition of LIRGs respectively. The diagonal dashed line shows $L_K \propto L_{\text{TIR}}$, and guides the eye for the radial dependence of $\langle L_K \rangle$ and $\langle L_{\text{TIR}} \rangle$ respectively, as shown by the color-coded filled circles – see legend.

4. Results

We identify 192 *Herschel* sources down to $L_{\text{TIR}} > 3 \times 10^{10} L_{\odot}$ and $L_K > 0.25 L_K^*$ (Fig. 2) within a clustercentric radius of $R < 1.5 r_{200}$ and lying inside the caustics in the velocity-radius plane (see Haines et al. 2010 for an example). Just $(24 \pm 3)\%$ ($46/192$) of these galaxies are LIRGs ($L_{\text{TIR}} > 10^{11} L_{\odot}$) and none are ultra-luminous IR galaxies (ULIRGs; $L_{\text{TIR}} > 10^{12} L_{\odot}$). The most luminous galaxy is the brightest cluster galaxy (BCG) in A 1835; we also detect the BCG in A 2390 (Edge et al. 1999; Egami et al. 2006). The typical galaxy has $L_K \approx 1.5 \times 10^{11} L_{\odot}$ and $L_{\text{TIR}} \approx 6 \times 10^{10} L_{\odot}$. On average, the most IR-luminous galaxies are found at projected cluster-centric radii of $\sim 1.5 r_{200}$; at larger and smaller radii the average IR-luminosity declines. This trend is mirrored by a decline in the average K -band luminosity such that $\langle L_{\text{TIR}}/L_K \rangle$ is conserved down to $\sim 0.5 r_{200}$, interior to which the average IR-luminous galaxy jumps from $\langle L_{\text{TIR}}/L_K \rangle (R \geq 0.5 r_{200}) \approx 0.39 \pm 0.03$ to $\langle L_{\text{TIR}}/L_K \rangle (R \leq 0.5 r_{200}) \approx 0.53 \pm 0.03$ (Fig. 2).

The S_{100}/S_{24} colors of the IR-detected galaxies have a prominent excess of flux at $100 \mu\text{m}$ relative to that expected from the commonly used Rieke et al. (2009) SED templates (Fig. 3). Adopting $S_{100}/S_{24} > 25$ as defining this unexpected red population, we find that $(63 \pm 4)\%$ ($121/192$) of the spectroscopically confirmed members are “red”, with $(78^{+6}_{-8}\%)$ ($36/46$) of LIRG members, and $(58^{+4}_{-5}\%)$ ($85/146$) of sub-LIRG members being “red” respectively. The predominance of red LIRGs is partly expected given the predicted relationship between luminosity and color, however the observed LIRGs lie almost exclusively red-ward of the Rieke et al. models. The fraction of galaxies with red colors also shows a gentle increase towards

the cluster centers: $f_{\text{red}} \propto R^{(-0.2 \pm 0.1)}$. The mean color of *Herschel*-detected cluster members, $\langle S_{100}/S_{24} \rangle = 29.2 \pm 0.1$, is also slightly redder than the mean color of *Herschel*-detected non-members (defined as lying outside the caustics, but within $0.15 < z < 0.3$), $\langle S_{100}/S_{24} \rangle = 27.0 \pm 0.1$. Both of these correlations point to a physical origin for these red colors, rather than systematic photometric errors. Indeed, Rawle et al. (2010) find a similar population in the core of the Bullet cluster. However the small difference between the color distributions of members and non-members suggest that cluster physics may not be the main determinant of the IR colors (see also Pereira et al. 2010).

The IR luminous population traces the structure of the mass distribution of the clusters and the surrounding filamentary structure, as traced by Ok10’s weak-lensing mass maps (Fig. 4). This is quantified using the number density of galaxies (normalized to the mean galaxy number density in each case) as a function of projected cluster mass density obtained from the mass maps (Fig. 4). A spatially random distribution of galaxies is consistent with unity; positive correlation between galaxies and mass is greater than unity, and anti-correlation is less than unity. We detect correlation between the spatial distribution of the IR luminous cluster members and the cluster mass distributions at $\sim 5\sigma$ significance.

We also combine the *Herschel* data with Ok10’s weak-lensing analysis to construct the first ever mass- L_{TIR} relation for galaxy clusters (Fig. 3), obtaining $L_{\text{TIR}} (< r_{\text{virial}}) \propto M_{\text{virial}}^{\alpha}$, with $\alpha = 1.9^{+1.4}_{-0.5}$. The fit was done taking into account errors in both variables, and was repeated 10^4 times, each time drawing 8 clusters at random with replacement; the error quoted on the slope is dominated by the scatter between these bootstrap samples. The mass-to-light ratio of a $\sim 10^{15} M_{\odot}$ cluster is $\sim 10^3 M_{\odot}/L_{\odot}$, however the scaling of mass with far-IR luminosity is inconsistent with a constant mass-to-light ratio at $\sim 2\sigma$.

Cluster IR luminosity density profiles, normalized to the underlying dark matter density profile from Ok10, are generally increasing functions of clustercentric radius out to at least r_{200} (Fig. 3). IR luminosity in excess of that expected from a flat mass-to-light ratio profile is therefore found at large clustercentric radii, particularly at $R \sim 1 - 1.5 r_{\text{virial}}$, where some of the profiles show a pronounced peak. We also note that strong-lensing clusters (A 1835, A 1689, A 2219, A 2390) tend to have steeper mass-normalized luminosity density profiles than non-strong-lensing clusters, three of which are well-known merging clusters (A 1763, A 1758, A 1914) in which the merger axis is likely close to the plane of the sky. Cluster geometry, e.g. prolate shape and/or merger aligned with the line of sight (strong-lensing clusters) versus aligned in the plane of the sky, therefore may complicate the detailed interpretation of the luminosity density profile shapes.

5. Summary and Discussion

We have presented an initial broad-brush analysis of *Herschel*/PACS observations of 25% of our sample of 30 galaxy clusters at $z \approx 0.2$, and combined these data with our existing *Spitzer*, Subaru, *Chandra*, UKIRT, and MMT data. The main analysis concentrates on a sample of 192 spectroscopically confirmed cluster members with $L_{\text{TIR}} > 3 \times 10^{10} L_{\odot}$, $L_K > 0.25 L_K^*$, $R < 1.5 r_{200}$. The average K -band luminosity of these galaxies fades by a factor of almost 2 from the cluster outskirts ($\sim 1 - 2 r_{200}$) to the cluster cores ($\leq 0.5 r_{200}$), although the average specific star-formation rate, as probed by $\langle L_{\text{TIR}} \rangle / \langle L_K \rangle$, is constant across most of this radial range ($\sim 0.5 - 2 r_{200}$), before

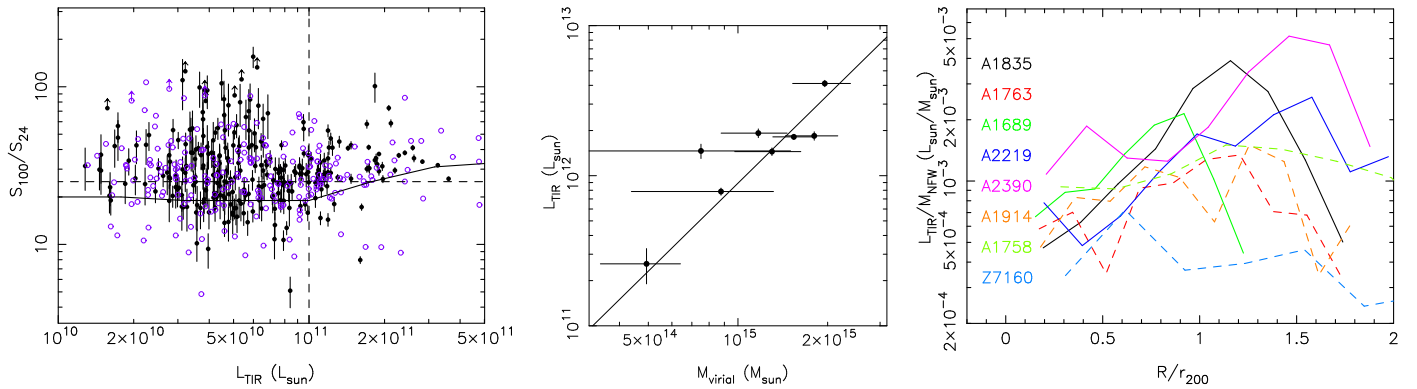


Fig. 3. **Left** – Far-IR color-luminosity relation; the color-luminosity relation predicted by the Rieke et al. (2009) SED templates is shown as the black solid line. The vertical and horizontal dashed lines mark the definition of LIRGs, and the nominal color cut discussed in §4, respectively. Cluster members are shown as filled black circles, and non-members as open purple circles. **Center** – Cluster virial mass versus bolometric infrared luminosity within the virial radius; the best-fit relation is shown as a solid line. **Right** – Total IR luminosity density profile relative to total mass density profile (§4). Strong-lensing clusters (Richard et al. 2010) are plotted as solid curves and non-strong-lensing clusters as dashed curves. The legend lists clusters from most (A 1835) to least (Z 7160) massive.

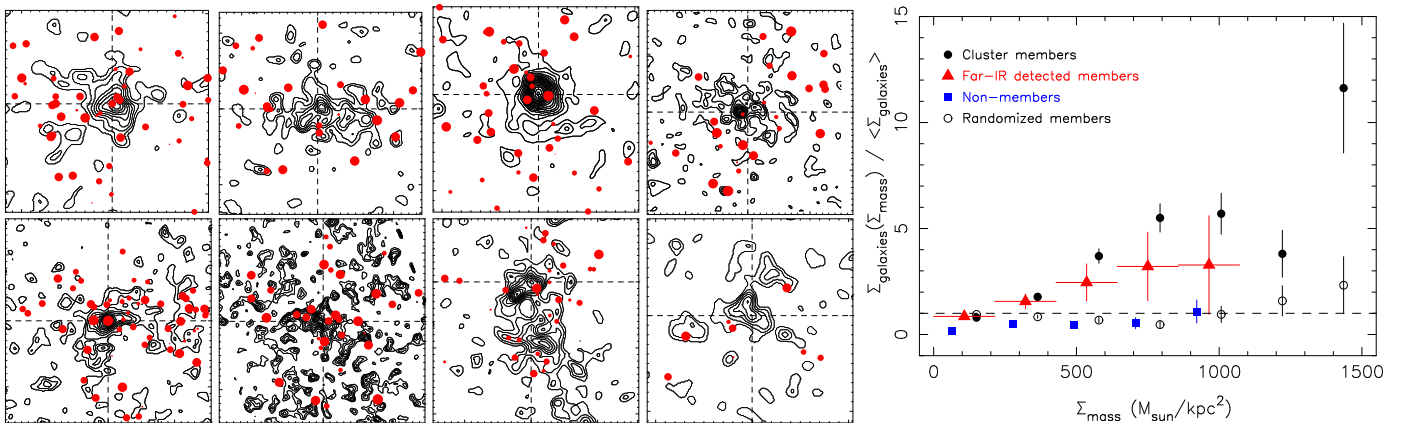


Fig. 4. **Left** – Weak lensing mass maps (contours, spaced at 1σ mass reconstruction error; Ok10; Okabe & Umetsu 2008) in order of decreasing cluster virial mass – top left-to-right: A 1835, A 1763, A 1689, A 2219; bottom: A 2390, A 1914, A 1758, Z 7160. Spectroscopically confirmed *Herschel*-detected members (selected as described in §4) are marked as filled red circles that scale logarithmically with L_{TIR}/L_K . North is up and East is left, and the axis tick-marks are spaced at 1 arcmin intervals. **Right** – Number density of galaxies relative to the mean number density of each population as a function of total projected cluster mass density. Positive correlation of the *Herschel*-detected cluster members with the mass distribution in/surrounding the clusters is detected at $\sim 5\sigma$. The absence of red triangular data points at $\Sigma_{\text{mass}} > 1000 M_{\odot} \text{kpc}^{-2}$ is because we do not find any non-BCG IR luminous cluster members at such high densities. The dip in the signal for cluster members at $\sim 1250 M_{\odot} \text{kpc}^{-2}$ is due to the incompleteness of our spectroscopic catalog in high density environments due to MMT/Hectospec fiber collisions.

jumping by 25% on smaller scales. This suggests that as gas rich galaxies fall into the clusters (typically in groups – Fig. 1) ongoing star-formation stops first in the most massive galaxies. As galaxies reach the cluster cores physical processes that operate in high density environments, for example ram pressure stripping and harassment, then appear to trigger a final episode of star-formation that presumably exhausts the remaining gas supply.

This picture is consistent with our comparison of the *Herschel*-detected cluster members with the cluster mass distributions, as probed by Okabe et al.’s (2010) weak-lensing analysis. First, the spatial distribution of the *Herschel* sources is positively correlated with the structures in the weak-lensing mass maps at $\sim 5\sigma$ significance, with the strongest signal seen at intermediate, group-like densities. Second, the strong dependence of the total cluster IR luminosity on cluster mass ($L_{\text{TIR}} \propto M_{\text{virial}}^2$) is

consistent with accretion of galaxies and groups of galaxies driving the cluster IR luminosity. This is because, assuming that IR galaxy mass-to-light ratios are independent of the cluster mass, the scaling relation can be understood as stemming from the M^2 dependence of the substructure mass function seen in theoretical models (e.g. Taylor & Babul 2005). Third, the IR luminosity density profiles of the clusters generally increase to large radii, with some clusters showing a peak at $\sim r_{200}$. This is qualitatively consistent with the enhanced star-formation rates seen in in-falling galaxy populations by Moran et al. (2005).

The most surprising result is that roughly half of the *Herschel*-detected cluster galaxies have excess flux at $100\mu\text{m}$ over that predicted from current SED models. Cluster members are redder than non-members, and we find a shallow trend of increasing fraction of red IR galaxies towards the cluster centers, both of which suggest that this is a physical effect and not caused

by systematic photometric uncertainties. This result will be the focus of more detailed future investigation.

Finally, we note that, contrary to previous speculation in the literature, we do not find a strong relationship between cluster IR luminosity and cluster dynamical state. Observations of the full sample will allow us to investigate this issue in more detail.

Acknowledgements. We acknowledge the anonymous referee for helping us to clarify various aspects of this letter. We thank our colleagues within the LoCuSS collaboration for many stimulating discussions, and their enthusiastic support. GPS is supported by the Royal Society. CPH and AJRS thank STFC for some support. Support for this work was provided by NASA through an award issued by JPL/Caltech. YYZ is supported by the German BMBF through the Verbundforschung under grant 50 OR 1005.

References

- Bai et al., 2009, *ApJ*, 693, 1840
 Böhringer et al., 2004, *A&A*, 425, 367
 Doyon & Joseph, 1989, *MNRAS*, 239, 347
 Dressler A., et al., 1997, *ApJ*, 490, 577
 Ebeling et al., 1998, *MNRAS*, 301, 881
 Ebeling et al., 2000, *MNRAS*, 318, 333
 Edge A.C., et al., 1999, *MNRAS*, 306, 599
 Egami E., et al., 2006, *ApJ*, 647, 922
 Fabricant D., et al., 2005, *PASP*, 117, 1411
 Fadda D., et al., 2008, *ApJ*, 672, 9
 Geach J., et al., 2006, *ApJ*, 649, 661
 Gunn & Gott, 1972, *ApJ*, 176, 1
 Haines C. P., et al., 2009, *MNRAS*, 396, 1297
 Haines C. P., et al., 2009, *ApJ*, 704, 126
 Haines C. P., et al., 2010, this volume
 Leggett S., et al., 1987, *MNRAS*, 228, 11
 Kodama T., et al., 2004, *MNRAS*, 354, 1103
 Lin Y., et al., 2004, *ApJ*, 610, 745
 McCarthy I., et al., 2008, *MNRAS*, 383, 593
 Metcalfe, et al., 2005, *SSRv*, 119, 425
 Miller et al., 2006, *AJ*, 131, 2426
 Moore B., et al., 1999, *MNRAS*, 304, 465
 Moran S. M., et al., 2005, *ApJ*, 634, 977
 Moran S. M., et al., 2006, *ApJ*, 641, 97
 Moran S. M., et al., 2007, *ApJ*, 671, 1503
 Okabe N. & Umetsu K., 2008, *PASJ*,
 Okabe N., et al., 2010, arXiv:0903.1103
 Ott, S., 2010, in ASP Conference Series, Astronomical Data Analysis Software and Systems XIX, Y. Mizumoto, K.-I. Morita, and M. Ohishi, eds., in press
 Pereira M. J., et al., 2010, this volume
 Pilbratt et al., 2010, this volume
 Poggianti B. & Wu, 2000, *ApJ*, 529, 157
 Pogtitsch, et al., 2010, this volume
 Popesso, P., et al., 2005, *A&A*, 433, 431
 Postman M., et al., 2005, *ApJ*, 623, 721
 Rawle T. D., et al., 2010, this volume
 Richard J., et al., 2010, *MNRAS*, 404, 325
 Rieke G. H., et al., 2009, *ApJ*, 692, 556
 Sanderson A. J. R., et al., 2009, *MNRAS*, 398, 1698
 Smith G. P., et al., 2005, *ApJ*, 620, 78
 Taylor & Babul, 2005, *MNRAS*, 364, 515

- ⁸ Center for Space Science Technology, University of Maryland Baltimore County, 1000 Hilltop Circle, Baltimore, MD 21250, USA
⁹ Academia Sinica Institute of Astronomy and Astrophysics, P.O. Box 23-141, 10617 Taipei, Taiwan
¹⁰ Institute of Computational Cosmology, University of Durham, South Road, Durham, DH1 3LE, England
¹¹ Institute for Physics & Mathematics of the Universe, University of Tokyo, 5-1-5 Kashiwa-no-Ha, Kashiwa City, 277-8582, Japan

¹ School of Physics and Astronomy, University of Birmingham, Edgbaston, B15 2TT, England. e-mail: gps@star.sr.bham.ac.uk

² Steward Observatory, University of Arizona, 933 North Cherry Avenue, Tucson, AZ85721, USA

³ Department of Physics and Astronomy, The Johns Hopkins University, 3400 N. Charles Street, Baltimore, MD 21218, USA

⁴ Rensselaer Polytechnic Institute (RPI) 110 Eighth Street, Troy, NY 12180, USA

⁵ Department of Physics and Astronomy, University of Victoria, 3800 Finnerty Road, Victoria, BC, Canada

⁶ Argelander-Institut für Astronomie, Universität Bonn, Auf dem Hügel 71, 53121 Bonn, Germany

⁷ Max-Planck-Institut für extraterrestrische Physik, Giessenbachstraße, 85748 Garching, Germany